

SPECTROSCOPIC CONFIRMATION OF THE EXISTENCE OF LARGE, DIFFUSE GALAXIES IN THE COMA CLUSTER

PIETER G. VAN DOKKUM¹, AARON J. ROMANOWSKY^{2,3}, ROBERTO ABRAHAM⁴, JEAN P. BRODIE³, CHARLIE CONROY⁵, MARLA GEHA¹, ALLISON MERRITT¹, ALEXA VILLAUME³, JIELAI ZHANG⁴

Draft version April 15, 2015

ABSTRACT

We recently identified a population of low surface brightness objects in the field of the $z = 0.023$ Coma cluster, using the Dragonfly Telephoto Array. Here we present Keck spectroscopy of one of the largest of these “ultra-diffuse galaxies” (UDGs), confirming that it is a member of the cluster. The galaxy has prominent absorption features, including the Ca II H+K lines and the G-band, and no detected emission lines. Its radial velocity of $c_z = 6280 \pm 120$ km/s is within the 1σ velocity dispersion of the Coma cluster. The galaxy has an effective radius of 4.3 ± 0.3 kpc and a Sersic index of 0.89 ± 0.06 , as measured from Keck imaging. We find no indications of tidal tails or other distortions, at least out to a radius of $\sim 2r_e$. We show that UDGs are located in a previously sparsely populated region of the size – magnitude plane of quiescent stellar systems, as they are ~ 6 magnitudes fainter than normal early-type galaxies of the same size. It appears that the luminosity distribution of large quiescent galaxies is not continuous, although this could largely be due to selection effects. Dynamical measurements are needed to determine whether the dark matter halos of UDGs are similar to those of galaxies with the same luminosity or to those of galaxies with the same size.

Keywords: galaxies: clusters: individual (Coma) — galaxies: evolution — galaxies: structure

1. INTRODUCTION

In the Spring of 2014 we obtained wide-field ($3^\circ \times 3^\circ$) observations of the Coma cluster with the Dragonfly Telephoto Array (Abraham & van Dokkum 2014). These images have low spatial resolution ($\approx 6''$), but reach surface brightness limits of $\mu(g) \sim 29.3$ mag arcsec⁻². We found a population of spatially-extended, low surface brightness objects in these images (van Dokkum et al. 2015). After combining the data with higher resolution imaging from the Sloan Digital Sky Survey (SDSS) and the Canada France Hawaii Telescope (CFHT), we identified 47 objects with effective radii in the range $r_e = 3'' - 10''$ and central surface brightness $\mu(g, 0) = 24 - 26$ mag arcsec⁻².

Based on the spatial distribution of the objects, and the smooth appearance of one of them in a deep *Hubble Space Telescope* Advanced Camera for Surveys image, we concluded that they are probably galaxies in the Coma cluster. The Coma cluster has a radial velocity of $c_z = 7090$ km s⁻¹ (Geller, Diaferio, & Kurtz 1999), and for a Hubble constant of 70 km s⁻¹ Mpc⁻¹ this implies a distance of ≈ 100 Mpc ($D_A = 98$ Mpc and $D_L = 103$ Mpc). This distance places the galaxies in an interesting region of parameter space: with effective radii of $r_{\text{eff}} = 1.5$ kpc – 4.6 kpc their sizes are similar to those of $\sim L_*$ galaxies, even though their luminosities, colors, axis ratios, and Sersic (1968) indices are similar to those of dwarf spheroidal galaxies. In van Dokkum et al. (2015) [vD15] we used the term “ultra-diffuse galaxies”, or UDGs, to distinguish these large, relatively round, diffuse objects from the general classes of dwarf galaxies and low surface bright-

ness galaxies.

Although it is plausible that most or all of the 47 galaxies are indeed Coma cluster members, this can only be confirmed with secure distance measurements. This is particularly important for the largest galaxies: it may be that only the galaxies with the smallest apparent sizes are at ~ 100 Mpc, and that the largest ones are considerably closer (see, e.g., Merritt, van Dokkum, & Abraham 2014). Here we present spectroscopy and imaging with the 10 m W.M. Keck Observatory of the largest galaxy in the vD15 sample, DF44. The goal of the spectroscopy is to test whether the galaxy is, in fact, in the Coma cluster. The imaging provides improved measurements of its morphology and structural parameters.

2. OBSERVATIONS AND REDUCTION

Galaxy DF44 ($\alpha = 13^{\text{h}}00^{\text{m}}58.0^{\text{s}}$; $\delta = 26^\circ 58' 35''$) was chosen because it is the largest (and second-brightest) galaxy in the sample of vD15. It has a major-axis effective radius of $9''.8$ and an integrated apparent magnitude of $m_g = 19.4$, as measured from CFHT images (see Fig. 1a).⁶ The effective radius was derived by fitting a 2D Sersic profile. The Sersic index was fixed to $n = 1$ (exponential) in this fit, as the S/N in the CFHT images is not sufficiently high to measure n reliably (see vD15). In Sect. 4 we update these measurements using deeper imaging from Keck. As shown in Fig. 1a, DF44 does not have bright neighbors. It is at a projected distance of $1''.04$ from the center of the cluster, corresponding to 1.8 Mpc or $\sim 0.6 \times R_{200}$ (Kubo et al. 2007).

The galaxy was observed 2014 December 18 and 19, using the Low Resolution Imaging Spectrometer (LRIS; Oke et al. 1995) on the Keck I telescope. Conditions were mostly clear. The 600 lines mm⁻¹ grism blazed at 4000 Å was used in the blue arm, and the gold-coated 1200 lines mm⁻¹ grating blazed

⁶ DF44 is also featured in Fig. 1 of vD15. A careful reader may note that the location of DF44 within the Coma field appears to be different in that paper. The apparent location of DF44 in vD15 is, indeed, incorrect; the red square in the Dragonfly image belongs to another one of the four highlighted galaxies.

¹ Department of Astronomy, Yale University, New Haven, CT 06511, USA

² Department of Physics and Astronomy, San José State University, San Jose, CA 95192, USA

³ University of California Observatories, 1156 High Street, Santa Cruz, CA 95064, USA

⁴ Department of Astronomy & Astrophysics, University of Toronto, 50 St. George St., Toronto, ON M5S 3H4 Canada

⁵ Harvard-Smithsonian Center for Astrophysics, 60 Garden St., Cambridge, MA, USA

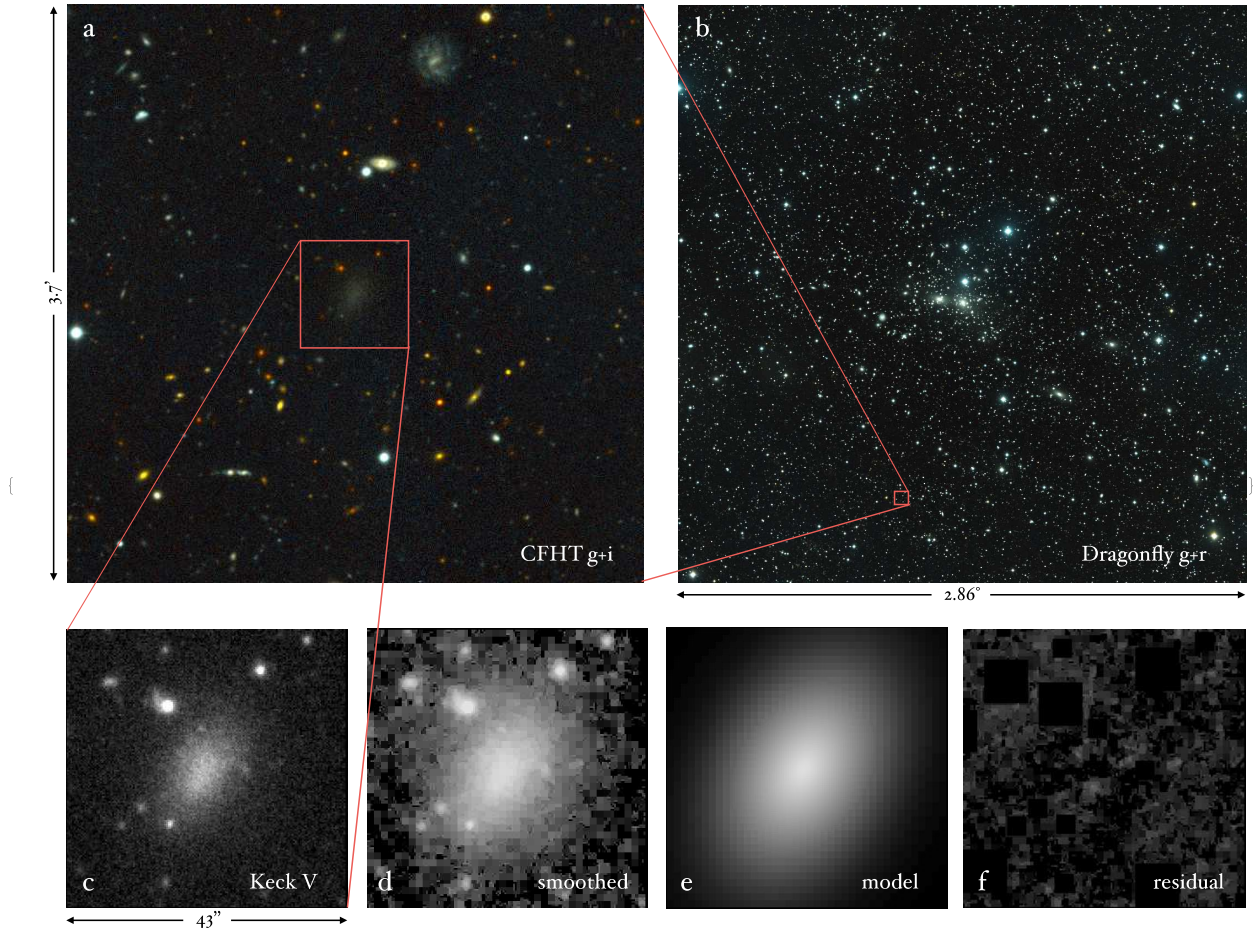


Figure 1. Imaging of DF44. Location of DF44 with respect to neighboring galaxies (a; CFHT image) and with respect to the center of the Coma cluster (b; Dragonfly discovery imaging). Panels c and d show the newly obtained Keck LRIS V -band image, before and after adaptive smoothing. Panels e and f show the best-fitting single component GALFIT model (Peng et al 2002) and the residual after subtracting this model from d.

at 9000 \AA in the red arm. With a $1''.5$ wide long slit, this configuration gives a spectral resolution of $\sigma_{\text{instr}} = 2.5 \text{ \AA}$ in the blue and $\sigma_{\text{instr}} = 0.85 \text{ \AA}$ in the red, corresponding to 170 km s^{-1} at $\lambda = 4500 \text{ \AA}$ and 30 km s^{-1} at $\lambda = 8500 \text{ \AA}$. The slit was approximately aligned with the major axis of the galaxy. The total integration time was 5400 s, divided over six exposures. The galaxy was moved along the slit in between exposures.

The blue and red spectra were reduced using standard techniques for long slit spectroscopy (see, e.g., van Dokkum & Conroy 2012, for an example using a similar instrumental setup as employed here). Sky OH emission lines were used for wavelength calibration and rectification in the red. In the blue, an arc spectrum taken immediately after the science exposures was used for this purpose. The wavelength coverage was $3065 \text{ \AA} - 5560 \text{ \AA}$ in the blue and $7590 \text{ \AA} - 9220 \text{ \AA}$ in the red. Sky subtraction was done by fitting a linear function in the spatial direction. The galaxy was masked in the fit. One-dimensional spectra were extracted by summing rows in the two-dimensional spectra. The extraction regions are $\approx 11''$, and correspond approximately to the rows where the flux is at least 30% of the peak. Extraction with optimal weighting, or using a smaller or larger aperture, does not improve the quality of the 1D spectrum. A relative flux calibration was ob-

tained using observations of the spectrophotometric standard Feige 110 (Hamuy et al. 1992).

We also obtained V band imaging of DF44, using the blue arm of LRIS. A total of 1080 s was obtained over the two nights, distributed over six dithered 180 s exposures. The data were reduced using standard techniques. In addition to a domeflat, a sky flat was used to correct for remaining variation in the background. As the galaxy was imaged on independent regions of the detector, the sky flat was created from the six science exposures themselves. The FWHM seeing in the final, combined image is $1''.0$. The image was calibrated using SDSS g and r photometry of stars in the DF44 field, using $V = g - 0.52(g - r) - 0.03$ (Jester et al. 2005).

3. REDSHIFT MEASUREMENT

The LRIS spectrum of DF44 is shown in Fig. 2. Only the blue side spectrum is shown, as the red spectrum has much lower signal-to-noise ratio (S/N) per resolution element. No absolute calibration of the spectrum was attempted, but the relative flux as a function of wavelength is correct to $\sim 10\%$ (as determined from the residuals between our calibrated spectrum of Feige 110 and the one in Hamuy et al. 1992). The spectrum resembles those of early-type galaxies: we unambiguously identify the Ca II H+K lines, the G-band at

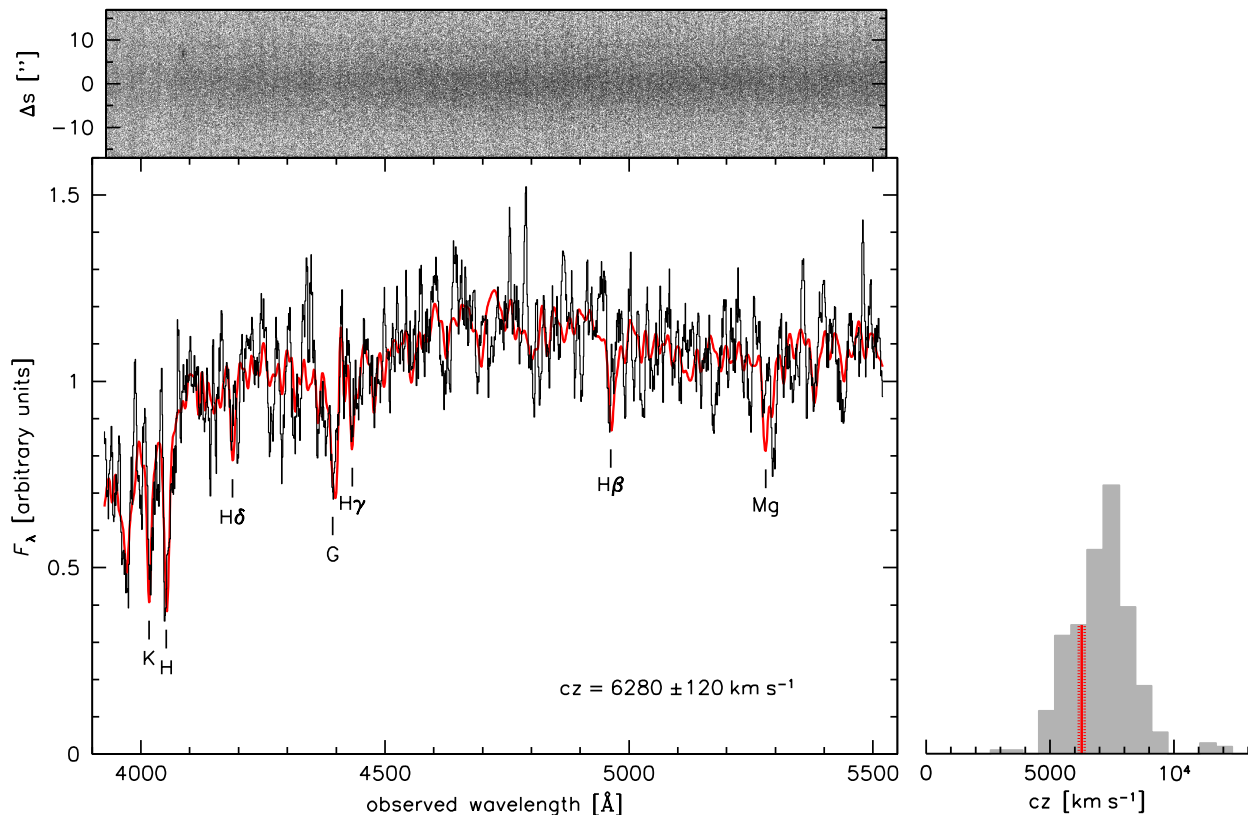


Figure 2. Spectrum of DF44, obtained in 5400 s with LRIS on the Keck I telescope. Top panel: two-dimensional spectrum. The left axis indicates the position along the slit, in arcseconds. Bottom panel: one-dimensional spectrum, extracted from the 2D spectrum (black line). The spectrum was smoothed with a 4.6 \AA box car filter. The red line shows the smoothed best-fitting model spectrum. The galaxy has an early-type spectrum, and a redshift of $cz = 6280 \pm 120 \text{ km s}^{-1}$. The histogram on the right shows the redshift distribution of Coma, from Mobasher et al. (2001). The red line marks the redshift of DF44.

4300 \AA , and several other metal lines. The Balmer lines $H\beta$, $H\gamma$, and $H\delta$ are also detected. No emission lines are found.

The redshift of DF44 was measured by cross-correlating the spectrum with a range of templates of stars and galaxies, obtained from the SDSS library.⁷ The best-fitting redshift is $cz = 6280 \pm 120 \text{ km s}^{-1}$. The redshift distribution in a 2.2 degree^2 region of the Coma cluster (Mobasher et al. 2001) is shown on the right. The mean redshift of the cluster is $cz = 7090 \text{ km s}^{-1}$ (Geller et al. 1999), with a dispersion of $\sim 1100 \text{ km s}^{-1}$ (e.g., Colless & Dunn 1996; Mobasher et al. 2001). We conclude that DF44 is a member of the Coma cluster and is located at a distance of $\approx 100 \text{ Mpc}$.

We also fitted the spectrum with the flexible stellar population synthesis (FSPS) models of Conroy, Gunn, & White (2009), using the methodology of Conroy & van Dokkum (2012). This fit simultaneously determines the best-fitting velocity dispersion, age, and metallicity, along with the redshift. Unfortunately, the S/N of the spectrum ($\approx 5 \text{ per \AA}$) is too low for stable constraints on these parameters, even when the elemental abundance ratios are fixed to the Solar values. The red line in Fig. 2 is the best-fitting FSPS model, after matching its continuum shape to that of DF44.

4. STRUCTURE

The Keck V band image of DF44 is shown in Fig. 1c. In Fig. 1d we show a version of the image that was smoothed

adaptively, to bring out the low surface brightness emission at large radii. This smoothing was done for display purposes only; the analysis was done on the original, unsmoothed image. We note that the Dragonfly image of DF44 (see vD15) reaches fainter surface brightness levels than the Keck image but is difficult to interpret due to confusion with neighboring objects. The galaxy has a regular, elliptical morphology, and there is no evidence for tidal features, spiral arms, or star forming regions, at least down to $\mu(V) \sim 28 \text{ mag arcsec}^{-2}$.

We fit elliptical isophotes to the image to measure the surface brightness profile and to determine whether there is evidence for isophotal twists or other irregularities. Prior to the fit, all other objects in the image were masked carefully. The sky background was determined from empty areas just outside of the region displayed in Fig. 1, and subtracted. The 1σ uncertainty in this background is approximately $\mu(V) \sim 29 \text{ mag arcsec}^{-2}$ and is propagated into the errors in the surface brightness profile.

The surface brightness profile of DF44 is shown in Fig. 3a. The surface brightness is approximately constant at $\mu(V) \approx 24.6 \text{ mag arcsec}^{-2}$ within $r = 3''$, and then falls off to reach $\mu(V) \approx 28 \text{ mag arcsec}^{-2}$ at $r = 20''$. The inner profile, highlighted in the inset, is influenced by the point spread function (PSF). We corrected the profile for the effects of the PSF following the procedure outlined in § 3 of Szomoru, Franx, & van Dokkum (2012). First, a 2D Sersic (1968) model, convolved with the PSF, was fitted to the image using GALFIT (Peng et al. 2002). Then, the residuals of this fit were added to

⁷ <http://www.sdss2.org/dr3/algorithms/spectemplates/index.html>

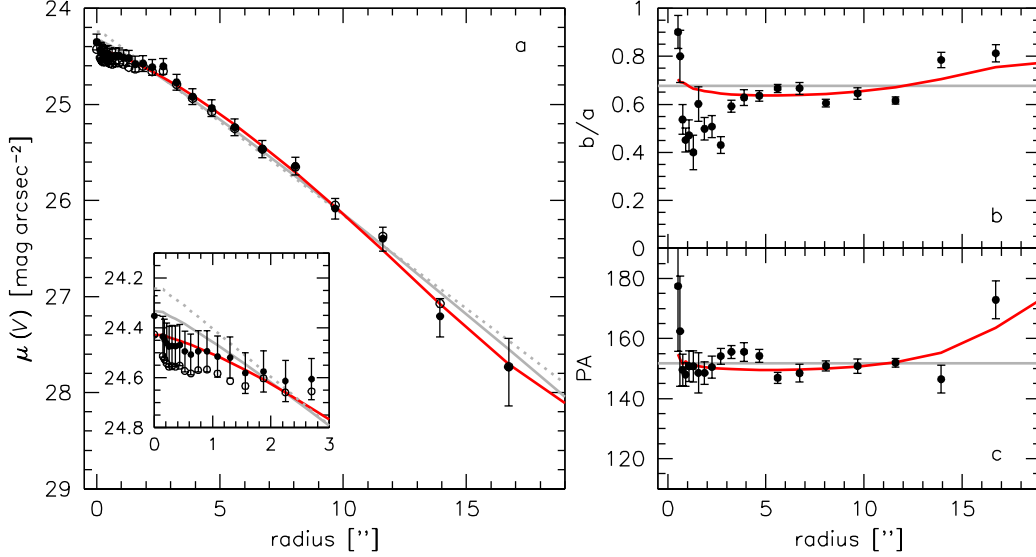


Figure 3. Surface brightness (a), axis ratio (b), and position angle (c) of DF44 as a function of distance along the major axis. Open symbols are the observed profile; solid symbols are corrected for the effects of the PSF (see text). In all panels the grey solid line is the best-fitting single component 2D Sersic model, with constant axis ratio and position angle. This model has a Sersic index $n = 0.9$ and an effective radius $r_e = 8''.9$, corresponding to 4.3 kpc at the distance of DF44. The grey broken line is an exponential fit, and the red line is a two-component fit. The two-component fit has an effective radius of $r_e = 8''.4$. The inset shows the inner part of the surface brightness profile. In the central $r < 3''$ ($r < 1.5$ kpc) the profile is depressed compared to the exponential fit.

an *unconvolved* 2D Sersic model, and the surface brightness profile was measured from this PSF-corrected image. The solid symbols in Fig. 3a show this PSF-corrected profile.

The grey line shows the best-fitting Sersic (1968) model. Note that this model has a constant ellipticity and position angle. It is a good fit to the observed profile: the rms in the difference between the solid points and the grey solid line is 0.08 magnitudes. The Sersic index of this model is $n = 0.89 \pm 0.06$, and the best-fitting effective radius is $r_e = 8''.9 \pm 0''.6$. At the distance of the Coma cluster of $D_A = 98$ Mpc this corresponds to $r_e = 4.3 \pm 0.3$ kpc. The total observed magnitude of the model is $m_V = 18.9$, and the absolute magnitude is $M_V = -16.1$. These results are consistent with our earlier measurement based on shallower CFHT data; specifically, if we force $n = 1$ we find $r_e = 4.5$ kpc, compared to $r_e = 4.6$ kpc from the CFHT data (vD15).

Panels b and c of Fig. 3 show the variation in the ellipticity and position angle as a function of radius. The radial variation in position is not shown, as the center of the best-fitting ellipse is always within $1''$ of the mean position. There is some evidence that the inner $r < 3''$ ($r < 1.5$ kpc) is structurally distinct from the rest of the galaxy: the surface brightness is depressed compared to an exponential model (broken grey line; this depression is why the best-fitting Sersic index is 0.9 rather than 1) and the galaxy appears more flattened (axis ratio $b/a \approx 0.5$ versus ≈ 0.7 at $r \gtrsim 5''$). The red line shows the result of a two-component GALFIT fit, with the Sersic index of the second component fixed to $n = 1$. The inner component has a Sersic index of $n = 0.69$, an effective radius of $r_{e,i} = 7''.5$, and an axis ratio $b/a = 0.57$; the outer component has $n \equiv 1$, $r_{e,o} = 14''.9$, and $b/a = 0.73$. The effective radius of the combined model is $8''.4$, very similar to that of the single-component fit.

5. DISCUSSION

The key result of this paper is the confirmation that one of the largest UDGs in the field of Coma is a member of the cluster. In vD15 we had already argued that the 47 diffuse ob-

jects we discovered with the Dragonfly Telephoto Array are very likely cluster members, but this was not based on direct distance measurements. The objects with the largest apparent sizes are most likely to be in the foreground, and by confirming the distance to DF44 we can be confident that most, and perhaps all, of the 47 galaxies are cluster members.

We note that this is not the first distance measurement to a large, diffuse galaxy. Caldwell (2006) measured the distance to even fainter (but also smaller) galaxies in the Virgo cluster from the location of the tip of the red giant branch. Dalcanton et al. (1997) measured redshifts of seven large field galaxies with central surface brightness in the range $\mu(V) = 23 - 25$ mag arcsec $^{-2}$. Two of these galaxies, R-127-1 and M-161-1, may be similar to DF44: they have no detected emission lines and they have similar sizes and surface brightness profiles. And XIX is the only known example of a faint galaxy with $r_e > 1.5$ kpc in the Local Group (McConnachie et al. 2008).

In Fig. 4 we place DF44 in context with these other UDGs, as well as with other classes of quiescent (i.e., not star forming) objects (see Brodie et al. 2011).⁸ The UDG data are taken from Table 1 in vD15, with $r_{e,circ} = (b/a)^{0.5} r_{e,maj}$. With $b/a = 0.68$, the circularized effective radius of DF44 is 3.5 kpc. Solid red lines indicate the approximate UDG selection limits of vD15, converted to the axes of Fig. 4: $r_{e,circ} > 1.3$ kpc and $\mu(V, 0) > 23.5$. The broken red line indicates the approximate detection limit of vD15 ($\mu(V, 0) \lesssim 25.5$; this is driven by the depth of the CFHT imaging that was used for confirmation). UDGs highlight the enormous range that exists in both axes of the size – luminosity diagram: at their magnitude they are a factor of > 100 larger than ultra-compact dwarfs and at their size they are a factor of > 100 fainter than normal elliptical galaxies. Interestingly all three classes of galaxies inhabit the same environments and have broadly similar stellar popula-

⁸ Most of the data in this figure come from the SAGES database (http://sages.ucolick.org/spectral_database.html).

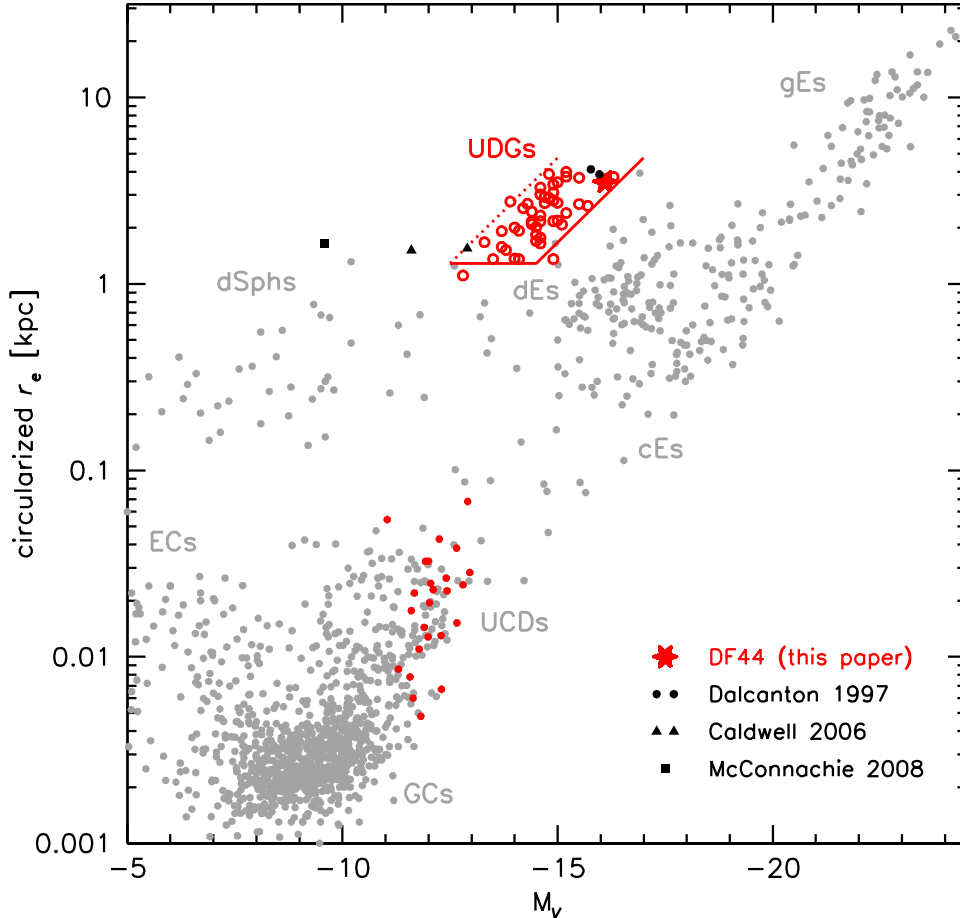


Figure 4. Relation between projected circularized half-light radius and absolute V band magnitude for quiescent (early-type) objects, adapted from Brodie et al. (2011). Solid symbols denote distance-confirmed objects. Red open circles are ultra-diffuse galaxies from vD15, assuming that they are all members of the Coma cluster. The solid star is DF44. The red lines indicate the approximate selection (solid) and detection (dotted) limits of vD15. Red solid circles are ultra-compact dwarfs in the Coma cluster (Chiboucas et al. 2011), which have a factor of $\sim 10^7$ higher 3D stellar density than the Coma UDGs. Black solid symbols are other diffuse galaxies with confirmed distances from the literature: the circles are the field galaxies R-127-1 and M-161-1 (Dalcanton et al. 1997), the triangles are the Virgo cluster galaxies N1sb10 and SW21sb31 (Caldwell 2006), and the square is the Local Group galaxy And XIX (McConnachie et al. 2008). The grey point near DF44 is the Virgo galaxy VCC 1661, which appears to be an erroneous measurement (McDonald et al. 2011).

tions. A striking feature of Fig. 4 is the apparent gap between the largest UDGs and giant elliptical galaxies of the same size (that is, there are very few quiescent galaxies with $r_e > 3$ kpc and $-20 < M_V < -17$). We caution, however, that the Brodie et al. sample was not designed to be complete in this domain, and that such objects would fall outside of the vD15 criteria.

The spectrum of DF44 does not provide new information on the formation of UDGs, beyond confirming that they have an early-type spectrum and no significant ongoing star formation. The deeper imaging enables us to address one particular explanation for the existence of UDGs, namely that they appear large because they have extensive tidal debris around them (see Koch et al. 2012, for a spectacular example of such a galaxy). Such tidal debris might be expected if UDGs are in the process of being disrupted by the tidal field of the cluster (e.g., Moore et al. 1996; Gnedin 2003). The Keck image of DF44 does not provide evidence for this scenario: the galaxy does not appear to be in the process of disruption, and the half-light radii are unlikely to be affected by tidal features. We note, however, that distortions may exist at fainter magnitudes.

The central depression in the surface brightness profile (relative to an exponential profile) is a common feature in dwarf spheroidal galaxies (Irwin & Hatzidimitriou 1995; McConnachie 2012; Merritt et al. 2014), and may be evidence of the importance of stellar feedback (e.g., Read & Gilmore 2005; Stinson et al. 2013). It may be that this feedback suppressed star formation at early times (see, e.g., Oppenheimer & Davé 2006; Scannapieco et al. 2008; Stinson et al. 2013), and that gas expelled in the associated winds was swept up in the intra-cluster medium (ICM) (e.g., Abadi, Moore, & Bower 1999; Mori & Burkert 2000) rather than falling back to the disk. In this scenario Coma UDGs could be considered “failed” $\sim L_*$ galaxies, that lost their gas to the ICM.

Key to understanding UDGs is to know how much dark matter they have, and, particularly, whether their halos resemble those of other galaxies of the same size or those of other galaxies of the same luminosity. The fact that UDGs are able to survive in the tidal field of Coma implies that they are dark matter-dominated (see vD15), but a quantitative mass measurement can only be obtained from internal kinematics. We calculate the expected stellar velocity dis-

person as a function of radius using simple spherical mass models with stars and Navarro, Frenk, & White (1997) dark matter halos, and a correlation between dark matter density and scale radius as in Spitler et al. (2012). If the dark matter halos of UDGs are similar to those of dwarf galaxies (with assumed $M_{\text{vir}} = 6 \times 10^{10} M_{\odot}$) their luminosity-weighted velocity dispersions are expected to be $\sim 35 \text{ km s}^{-1}$ within the stellar effective radius. By contrast, if their halos are similar to those of L_* galaxies (with assumed $M_{\text{vir}} = 1.8 \times 10^{12} M_{\odot}$), their dispersions are $\sim 60 \text{ km s}^{-1}$.⁹ In this paper we have shown what can be achieved in 1.5 hrs with a traditional long-slit spectrograph on a large telescope. Using long exposure times with

low surface brightness-optimized integral field units (such as the planned Keck Cosmic Web Imager; Martin et al. 2010), it should be possible to measure dynamical masses, ages, and metallicities of these enigmatic objects.

We thank Nicola Pastorello for an independent check of the redshift measurement. Support from NSF grants AST-1312376, AST-1109878, and AST-1211995 is gratefully acknowledged. We also acknowledge the support of the Dunlap Institute, funded through an endowment established by the David Dunlap family and the University of Toronto.

REFERENCES

- Abadi, M. G., Moore, B., & Bower, R. G. 1999, MNRAS, 308, 947
 Abraham, R. G. & van Dokkum, P. G. 2014, PASP, 126, 55
 Brodie, J. P., Romanowsky, A. J., Strader, J., & Forbes, D. A. 2011, AJ, 142, 199
 Caldwell, N. 2006, ApJ, 651, 822
 Chiboucas, K., Tully, R. B., Marzke, R. O., Phillipps, S., Price, J., Peng, E. W., Trentham, N., Carter, D., et al. 2011, ApJ, 737, 86
 Colless, M. & Dunn, A. M. 1996, ApJ, 458, 435
 Conroy, C., Gunn, J. E., & White, M. 2009, ApJ, 699, 486
 Conroy, C. & van Dokkum, P. 2012, ApJ, 747, 69
 Dalcanton, J. J., Spergel, D. N., Gunn, J. E., Schmidt, M., & Schneider, D. P. 1997, AJ, 114, 635
 Geller, M. J., Diaferio, A., & Kurtz, M. J. 1999, ApJ, 517, L23
 Gnedin, O. Y. 2003, ApJ, 589, 752
 Hamuy, M., Walker, A. R., Suntzeff, N. B., Gigoux, P., Heathcote, S. R., & Phillips, M. M. 1992, PASP, 104, 533
 Irwin, M. & Hatzidimitriou, D. 1995, MNRAS, 277, 1354
 Jester, S., Schneider, D. P., Richards, G. T., Green, R. F., Schmidt, M., Hall, P. B., Strauss, M. A., Vanden Berk, D. E., et al. 2005, AJ, 130, 873
 Koch, A., Burkert, A., Rich, R. M., Collins, M. L. M., Black, C. S., Hilker, M., & Benson, A. J. 2012, ApJ, 755, L13
 Kubo, J. M., Stebbins, A., Annis, J., Dell'Antonio, I. P., Lin, H., Khiabani, H., & Frieman, J. A. 2007, ApJ, 671, 1466
 Martin, C., Moore, A., Morrissey, P., Matuszewski, M., Rahman, S., Adkins, S., & Epps, H. 2010, in Society of Photo-Optical Instrumentation Engineers (SPIE) Conference Series, Vol. 7735, Society of Photo-Optical Instrumentation Engineers (SPIE) Conference Series, 0
 McConnachie, A. W. 2012, AJ, 144, 4
 McConnachie, A. W., Huxor, A., Martin, N. F., Irwin, M. J., Chapman, S. C., Fahlman, G., Ferguson, A. M. N., Ibata, R. A., et al. 2008, ApJ, 688, 1009
 McDonald, M., Courteau, S., Tully, R. B., & Roediger, J. 2011, MNRAS, 414, 2055
 Merritt, A., van Dokkum, P., & Abraham, R. 2014, ApJ, 787, L37
 Mobasher, B., Bridges, T. J., Carter, D., Poggianti, B. M., Komiyama, Y., Kashikawa, N., Doi, M., Iye, M., et al. 2001, ApJS, 137, 279
 Moore, B., Katz, N., Lake, G., Dressler, A., & Oemler, A. 1996, Nature, 379, 613
 Mori, M. & Burkert, A. 2000, ApJ, 538, 559
 Navarro, J. F., Frenk, C. S., & White, S. D. M. 1997, ApJ, 490, 493
 Oke, J. B., Cohen, J. G., Carr, M., Cromer, J., Dingizian, A., Harris, F. H., Labrecque, S., Lucinio, R., et al. 1995, PASP, 107, 375
 Oppenheimer, B. D. & Davé, R. 2006, MNRAS, 373, 1265
 Peng, C. Y., Ho, L. C., Impey, C. D., & Rix, H.-W. 2002, AJ, 124, 266
 Read, J. I. & Gilmore, G. 2005, MNRAS, 356, 107
 Scannapieco, C., Tissera, P. B., White, S. D. M., & Springel, V. 2008, MNRAS, 389, 1137
 Sersic, J. L. 1968, Atlas de galaxias australes (Cordoba, Argentina: Observatorio Astronomico, 1968)
 Spitler, L. R., Romanowsky, A. J., Diemand, J., Strader, J., Forbes, D. A., Moore, B., & Brodie, J. P. 2012, MNRAS, 423, 2177
 Stinson, G. S., Brook, C., Macciò, A. V., Wadsley, J., Quinn, T. R., & Couchman, H. M. P. 2013, MNRAS, 428, 129
 Szomoru, D., Franx, M., & van Dokkum, P. G. 2012, ApJ, 749, 121
 van Dokkum, P. G., Abraham, R., Merritt, A., Zhang, J., Geha, M., & Conroy, C. 2015, ApJ, 798, L45
 van Dokkum, P. G. & Conroy, C. 2012, ApJ, 760, 70

⁹ In either scenario the *stellar* mass does not contribute to the mea-

sured dispersion; the stars-only expectation for the velocity dispersion is $\sim 7 \text{ km s}^{-1}$, for $M_{\text{stars}}/L_V = 1.3$.